# Spectroscopic Analysis of Single-Walled Carbon Nanotubes and Semiconjugated Polymer Composites

**S. M. Keogh,* T. G. Hedderman, E. Gregan, G. Farrell, G. Chambers, and H. J. Byrne**

*Facility for Optical Characterisation and Spectroscopy (FOCAS)/School of Physics, Dublin Institute of Technology, Kevin Street, Dublin 8, Ireland*

*Received: October 1, 2003; In Final Form: March 10, 2004*

Interactions between arc discharge single-walled carbon nanotubes within polymer composites have been well documented. Here hybrid systems of the conjugated organic polymer poly(*p*-phenylene vinylene-*co*-2,5-dioctyloxy-*m*-phenylene vinylene) (PmPV) and HiPco SWNTs are explored using UV/vis/NIR and Raman spectroscopy at 514.5 and 632.8 nm to determine specific interactions. An examination of the radial breathing modes at 514.5 nm shows similar tube diameters of 1.28 and 1.35 nm selected for both the arc discharge and HiPco composites. The corresponding G lines of both composites show no specific type of tubes being selected. At 514.5 nm, the G line of the HiPco composite (1% mass fraction) shows contributions from semiconducing and metallic tubes, and the arc discharge composite (1% mass fraction) is dominated by semiconducting nanotubes. At 632.8 nm, the G line of the HiPco composite (1% mass fraction) is dominated by semiconducting tubes, and the arc discharge composite (1% mass fraction) shows strong contributions from metallic tubes. This finding is a strong indication that the selection process is dependent on tube diameter rather than backbone structure. The solubility limits of both composites are determined by investigating the G lines of both composites and have been found to be greater than 1% mass fraction by weight for the arc discharge composite and greater than 0.1% mass fraction by weight for the HiPco composite.

## 1. Introduction

Single-walled carbon nanotubes (SWNTs) exhibit many unique physical and chemical properties.[1,2] Although there are many production methods for SWNTs, none have been successful in producing 100% pure SWNTs in large quantities. Methods include laser vaporization of metal-doped targets,[3] arc discharge of metal-doped carbon electrodes,[4] and the most successful process to date, the gas-phase catalytic process, which produces high-purity HiPco SWNTs.[5,6] Nanotube characteristics are defined by how they are produced. Characteristics include electronic properties, diameter distribution, percentage purity, and type of impurity present. These factors affect the type of composites they form. Specific interactions between arc discharge SWNTs within polymer composites have been well documented.[7−15] One proposed system for purification uses the organic semiconjugated polymer poly(*p*-phenylene vinylene-*co*-2,5-dioctyloxy-*m*-phenylene-vinylene) (PmPV).[7] The chemical structure of PmPV has been shown to allow solubility because of the presence of floppy side chains and conjugation along the polymers' backbone.[8] The PmPV backbone reorganizes into a relatively flat helical structure because of the *m*-phenelylene linkage and repulsive interaction between the octyloxy groups.[8] Panhius et al. have shown that the exposure of the backbone plays an important role in facilitating dipolar binding between the polymer and the nanotube, allowing the polymer to $\pi$ stack onto the nanotube backbone.[9] The trans linkage is of particular importance in the repeat unit that inhibits polymer aggregation because all cis conformations have been shown to cause polymer aggregation and inhibit interaction with the nanotube.[10] Coleman et al. have proposed that the polymer is not binding over its entire length but that only a section of it is attached, with some 13 to 14 carbon atoms binding per molecule.[11] This is contradictory to wrapping the polymer around the nanotube in a periodic and well-defined manner, which was formerly thought to be the case.[12] The solubility limits of the arc disharge tubes within PmPV composites have been shown to be in the region of 2 wt %.[7] This polymer has been shown to interact with arc discharge tubes in the diameter range of 1.3−1.5 nm.[7] The aim of this work is to investigate whether PmPV will solubulize and interact with nanotubes synthesized by different methods. In this study, HiPco SWNT composites are compared to arc discharge composites to further elucidate this interaction. Nanotubes produced by these methods were chosen because arc discharge nanotubes are predominantly metallic under given conditions[16] and HiPco nanotubes show semiconducting contributions.[17] They both exhibit a different diameter range with different impurities as well as different production yields.[18] In this article, near-infrared and Raman spectra are presented. The results indicate that although both tubes have a different diameter distribution similar diameter ranges are selected. A resonant Raman investigation of the HiPco composite G line indicates that PmPV is not prejudiced toward tube type because both metallic and semiconducting tubes are selected at 514.5 nm. At 632.8 nm, the HiPco composite is dominated by semiconducting tubes compared to the arc discharge composite, which shows metallic contributions. This suggests that PmPV is more diameter-selective than tube-type-selective.

## 2. Materials Preparation

The arc discharge SWNTs used in this study were synthesized using the procedure outlined in ref 18. The HiPco SWNTs were obtained from Houston-based Nanotechnologies and are prepared as in ref 5. Composites of HiPco SWNTs (0.01, 0.1, and

* Corresponding author. E-mail: sinead.keogh@dit.ie.

10.1021/jp0369387 CCC: $27.50 
Published on Web 04/22/2004

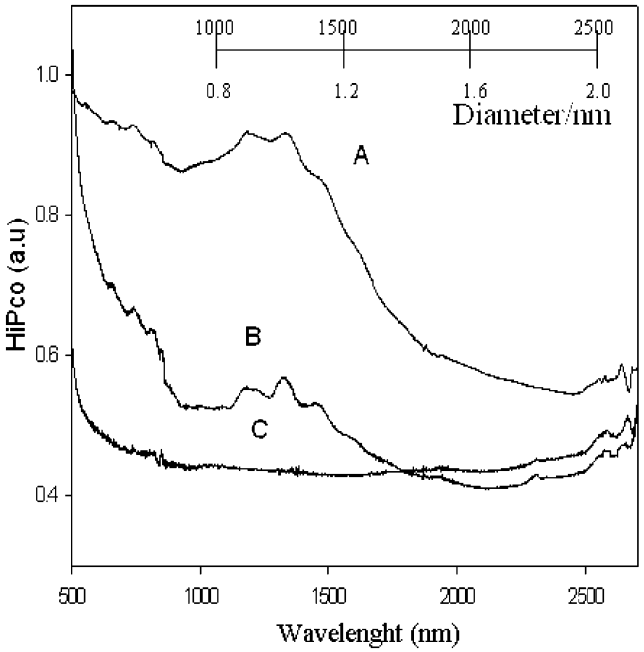


**Figure 1.** (A) NIR spectrum of HiPco SWNTs, (B) 1% HiPco/PmPV composite, and (C) pristine PmPV. The inset shows the relationship between diameter and wavelength.

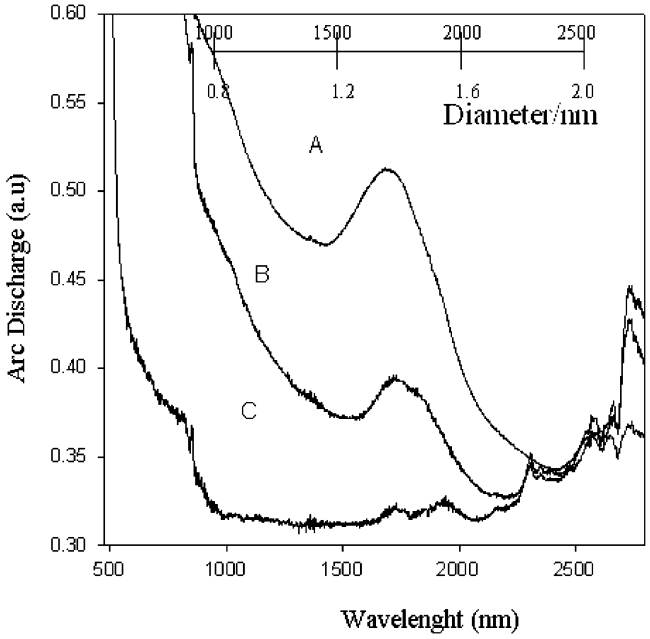


**Figure 2.** (A) NIR spectrum of raw arc discharge SWNTs, (B) the 1% arc discharge/PmPV composite, and (C) the 0.1% arc discharge/PmPV composite. The inset is the same as in Figure 1.

1 wt %) and arc discharge SWNTs (0.01, 0.1, and 1 wt %) were mixed in 1 g/L solutions of PmPV in toluene. The composites were sonicated for 11 h and left to stand for 48 h to allow amorphous carbon to precipitate to the bottom. The supernatant was pipetted, and thin films were prepared by drop casting onto glass slides. Raman spectra were obtained using an Instruments SA LabRam 1B system. This confocal imaging system uses either a He−Ne laser at 632.8 nm or an argon ion source at 514.5 nm. Samples were drop cast onto quartz slides for near-infrared spectra that were obtained using a Perkin-Elmer Lamda 900 UV/vis/NIR spectrometer.

### 3. Results and Discussion

Optical absorption spectroscopy has been shown to probe the electronic properties of SWNTs.[19,20] Because of the 1D character of SWNTs, van Hove singularities exist in the electronic density of states. An inversely proportional relationship between the intraband transitions and the diameter has been established for individual tubes.[21] Because of the polydiversity of the raw tube samples, the NIR spectrum is broad and can be used to determine the diameter distribution within samples. Van Hove singularities are observed in the NIR region for SWNTs, specifically in the 1800-, 1000-, and 700-nm regions.[19] Peaks at 1800 and 1000 nm have been assigned to semiconducting nanotubes, and peaks at 700 nm have been assigned to metallic nanotubes.[19] The raw arc discharge and HiPco tubes were characterized using UV/vis/NIR spectroscopy. Figure 1 presents absorption spectra of the raw HiPco SWNT (A), the 1% HiPco/PmPV composite (B), and PmPV (C). Figure 2 presents absorption spectra of the raw arc discharge SWNT (A), the 1% arc discharge/PmPV composite (B), and the 0.1% arc discharge PmPV composite (C).

In Figure 1, the raw HiPco sample shows distinct features ranging from 920 to 1875 nm, giving a diameter distribution of about 0.73 to 1.5 nm, with a mean diameter of 1.15 nm. This diameter distribution is in agreement with previous UV/vis/NIR spectra of HiPco tubes.[6,20,22] The most dominant peaks present consist of diameters of 0.95, 1.1, and 1.2 nm in the raw sample. A relatively flat PmPV spectrum is shown in curve C; as expected, no optical transitions occur in this region. The 1% HiPco composite is more defined with distinct features compared to the raw HiPco sample showing refinement in the diameter distribution of nanotubes present in the composite. Here, the diameter distribution has been reduced from 0.8 to 1.35 nm. Nanotubes in the region of 1.15 nm have become more resolved, with tubes of 0.95- and 1.1-nm still dominating the spectrum. It is worth noting that no shifting of peaks has been observed. In Figure 2, a broad feature appears in the raw arc discharge spectrum between 1380 and 2100 nm, giving a diameter distribution of about 1.1 to 1.74 nm, with the most dominant peak occurring at a diameter of 1.4 nm. This is in agreement with previous UV/vis/NIR studies on arc discharge tubes.[22,18] The broad featureless nature of the arc discharge profile in comparison to the highly resolved structure of HiPco may reflect the larger number of tubes that exist in the diameter region from 1.1 to 1.74 nm compared to the number that exist in the region from 0.73 to 1.5 nm.[19,20] It has furthermore been proposed that the fine structure of the raw HiPco spectrum can be attributed to the smaller average tube diameter present, compared to that of arc discharge, which may convey more structural information.[20] The 1% arc discharge composite shows that the fwhm has been reduced to a diameter distribution of 1.24 to 1.6 nm, showing a degree of selectivity. The dominant nanotube peak still occurs at 1.4 nm with a shoulder occurring at 1.45 nm. As the mass fraction is decreased further to 0.1%, it can be seen that this feature has become doubly split with nanotubes of diameters 1.4- and 1.5-nm dominating the spectrum. At 0.1% mass fraction, the diameter distribution has been reduced from 1.32 to 1.6 nm. The UV/vis/NIR spectrum clearly shows that HiPco selects smaller tubes compared to arc discharge, which selects larger tubes; however, for both tube types, the distributions overlap, and a similar diameter range of 1.24 to 1.35 nm is selected.

To examine the composites further, Raman spectroscopy was carried out at 514.5 and 632.8 nm. Two modes dominate the Raman spectrum of SWNTs. The first is the G line, which is strongly related to the tangential mode in graphite and occurs

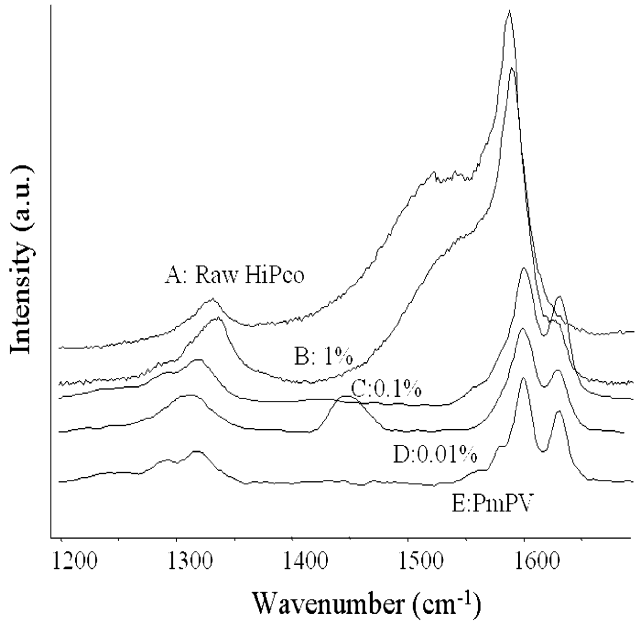


**Figure 3.** Raman spectra at 514.5 nm of various mass fractions of the HiPco composite.

around 1580 $cm^{-1}$. Because of nanotube curvature and the folding of the graphite Brillouin zone into the nanotube zone, the G band contains several modes with different symmetries that are Raman-active, including $A_{1g}$, $E_{1g}$, and $E_{2g}$.[23,24] Polarized Raman studies of individual SWNTs have shown four intrinsic Lorentzian components for the G line of semiconducting tubes, including 1549 $cm^{-1}$ [$E_2(E_{2g})$], 1567 $cm^{-1}$ [$A(A_{1g}) + E_1(E_{1g})$], 1590 $cm^{-1}$ [$A(A_{1g}) + E_1(E_{1g})$], and 1607 $cm^{-1}$ [$E_2(E_{2g})$].[25] The Raman spectra for metallic nanotubes in SWNT bundles exhibit only two peaks, including a higher-frequency mode that has a Lorentzian line shape and a lower-frequency mode that exhibits a Breit−Wigner−Fano (BWF) line shape.[26,27] The BWF line position has been shown to be diameter-dependent where the splitting of the G band increases with decreasing diameter[28,29] and the BWF line intensity increases with bundle thickness.[30,31]

The second originates from the radial breathing mode between 140 and 220 $cm^{-1}$ whose position and shape is related to the resonant enhancement of certain tubes at the wavelength of the excitation laser, which has been demonstrated by Rao et al.[21] Ab initio calculations have confirmed the inverse diameter dependence of the RBM frequency and have yielded an appropriate factor of proportionality, which is discussed later.[32,33] Thus, Raman has become a useful tool for the assignment and analysis of tube diameters within samples. Figure 3 presents the vibrational spectra at laser excitation 514.5 nm of the raw HiPco sample. Because of the diameter range of the sample (0.73−1.5 nm), both metallic and semiconducting tubes are resonant at this wavelength, and this has been shown previously.[34] This broad G line exhibits a slow decay back to the spectral baseline and is composed of a BWF at 1525 $cm^{-1}$, which is close to previous assignments for metallic tubes at 1522 $cm^{-1}$ at this excitation wavelength.[34] Also present are modes at 1594 and 1563 $cm^{-1}$ which can be attributed to semiconducting tubes.[25] This broadness has been attributed to the presence of metallic tubes[27] as well as the large diameter range of the sample as seen earlier in Figure 1 in the UV/vis/NIR spectrum. The vibrational spectroscopy of PmPV has been well explored.[35,36] In Raman, the pristine polymer spectrum as shown in Figure 3 is dominated by multiple modes around 1600 $cm^{-1}$.[37,38] There are at least four distinct modes in this feature, with the dominant one centered at 1592 $cm^{-1}$. These have been assigned to stretches within the phenyl ring.[38] The mode at 1631 $cm^{-1}$ has been attributed to the vinyl stretch on the backbone and is common to most PPV-based polymers.[38] Modes are also present at 1580 and 1559 $cm^{-1}$ in the pristine polymer spectrum. The 1% HiPco composite fwhm has decreased and has also shifted by 7 $cm^{-1}$ to 1590 $cm^{-1}$. This decrease in the fwhm is due to the decreased range in the diameters present at the 1% mass fraction (0.8−1.35 nm), which is also seen in the UV/vis/NIR spectrum. Modes present at 1590 and 1554 $cm^{-1}$ dominate the spectrum and have been assigned to semiconducting tubes,[25,27] although strong contributions from metallic tubes can be seen because of the broadness of the composite G line and the presence of a BWF line shape at 1535 $cm^{-1}$.[26] A new peak occurs at 1627 $cm^{-1}$, which is not present in the raw HiPco spectrum and is due to the presence of the polymer. As the mass fraction is decreased further to 0.1 and 0.01%, the G line fwhm has been reduced significally and has become more polymerlike, shifting to 1600 $cm^{-1}$. The peak at 1627 $cm^{-1}$ becomes more dominant in the 0.1 and 0.01% composite spectra compared to that in the 1% composite spectrum, and there is little evidence of metallic tubes present. A new peak at 1445 $cm^{-1}$ is present in the 0.01% composite, and this peak does not appear dominant at any other loading fraction. The origin of this peak is unknown, although it has also been observed in composites of arc discharge tubes and small organic molecules.[39] It is possibly an IR-active mode, which is activated in the Raman spectrum because of composite binding. It is clear that the introduction of nanotubes into the pristine polymer increasingly overshadows the polymer spectrum as the mass fraction of tubes is increased. This has been reported previously for arc discharge polymer composites.[7,15] The authors suggest that at low loading fractions the polymer intercalcates between nanotubes, which may lead to an unraveling of ropes.[15] This postulation has been used to explain the observed narrowing of the G line, which is due to a decreased interaction between the individual tubes.[7,15] The greatest change and shift in the G line occurs from the 0.1 to the 1% mass fraction. Here, the 0.1% composite loses its shoulder at 1500 $cm^{-1}$ and undergoes a shift of 12 $cm^{-1}$ to lower frequencies. This would suggest that perhaps the solubility limits for HiPco tubes occur between 0.1 and 1% loading fractions because modifications to the HiPco spectrum are greatest at 0.1% and above this loading the nanotubes are capable of reaggregating.

In Figure 4, the corresponding arc discharge composite spectra are presented. The larger-diameter-distribution (1.1−1.74 nm) SWNTs exhibit a predominantly semiconducting line shape at this wavelength in aggreement with resonance Raman theory and other work.[34] The raw arc discharge spectrum has a distinct G line present at 1584 $cm^{-1}$ and shoulders present at 1559 and 1591 $cm^{-1}$. We note that the fwhm of the raw arc discharge spectrum is considerably less than that of the raw HiPco spectrum. This would suggest that there are fewer arc-discharge-diameter tubes resonant at 514.5 nm compared to the number of HiPco tubes at the same excitation wavelength. This is reflected in the corresponding RBM spectra for the arc discharge tubes in Figure 8. Like the HiPco composite, the 1% arc discharge composite also has a shoulder at 1627 $cm^{-1}$ and has shifted by 7 $cm^{-1}$. Modes at 1569, 1590, and 1605 $cm^{-1}$ are also present and can be assigned to semiconducting tubes.[25,27] The 0.1% sample presents two distinct modes at 1592 and 1568 $cm^{-1}$. The shoulder at 1627 $cm^{-1}$ is no longer apparent. This 0.1% arc discharge spectrum is considerably more tubelike than the 0.1% HiPco spectrum. As the mass fraction is reduced to 0.01%, the spectrum clearly resembles the pristine polymer

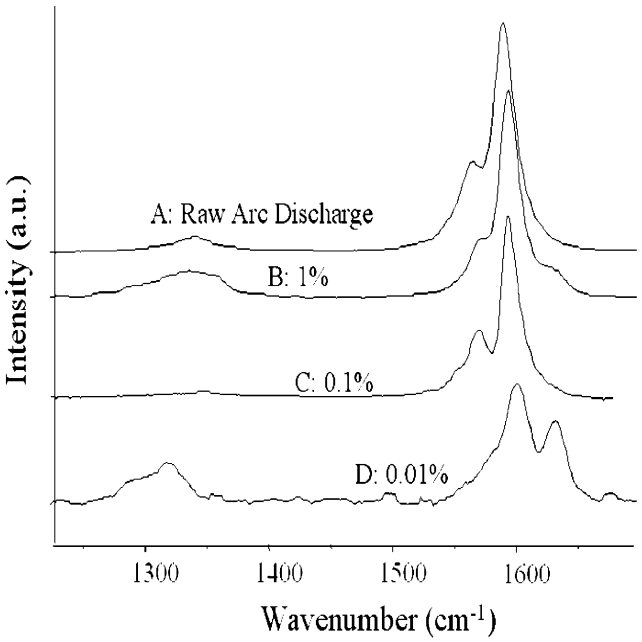


**Figure 4.** Raman spectra at 514.5 nm of various mass fractions of the arc discharge composite.

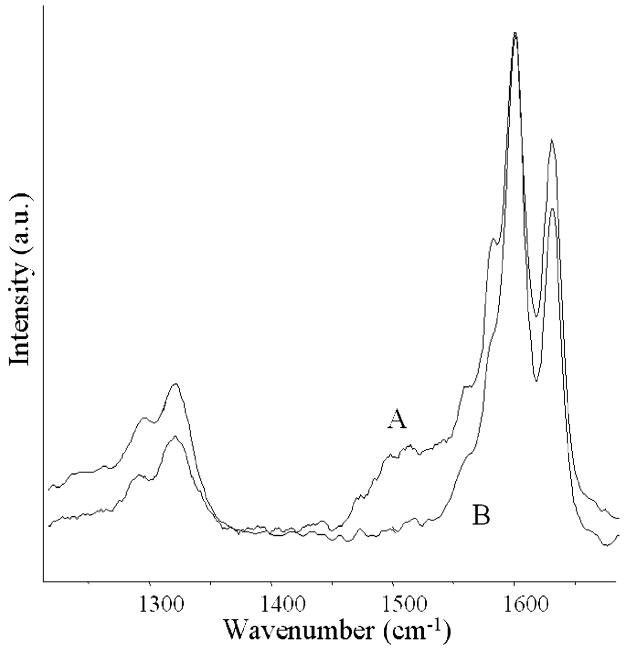


**Figure 5.** Raman spectra at 514.5 nm of (A) the combined HiPco and pristine polymer and (B) the 0.1% HiPco composite.

spectrum in Figure 3 although the peak at 1568 $cm^{-1}$ is not as dominant. The downshifting that occurs between the 1% sample and the raw sample would again suggest that the arc discharge tubes are soluble at a mass fraction greater than 1% because no observable shifts are seen below this mass fraction. This would suggest that arc discharge tubes are more soluble than HiPco tubes, but this is not necessarily the case because there are more tubes in a 1% mass fraction of HiPco composite compared to a 1% mass fraction of arc discharge composite. This is due to the fact that arc discharge tubes contain about 70% (by weight) impurities[4] compared to HiPco, which is about 90% (by weight) pure.[5,6] The polymer and nanotube spectra were mathematically combined to determine if downshifting in the composite spectra was due to this. Figure 5 presents the combination of raw HiPco and PmPV (A) and the 0.1% HiPco composite (B). Although

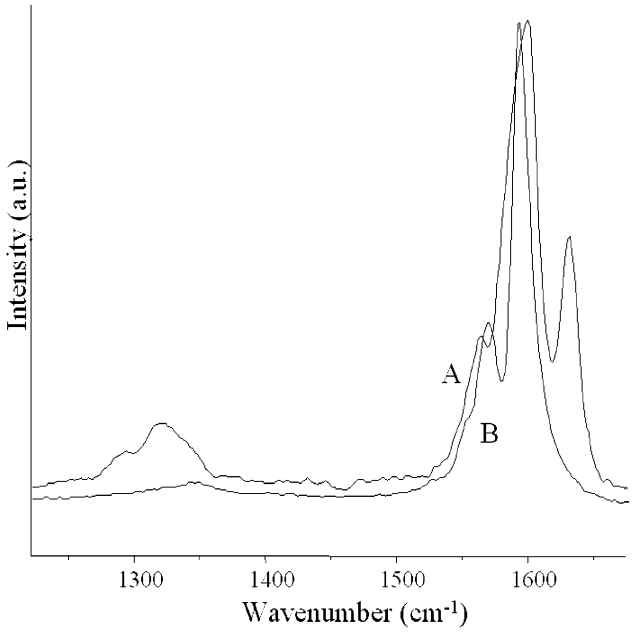


**Figure 6.** Raman spectra at 514.5 nm of (A) the combined arc discharge and pristine polymer and (B) the 0.1% arc discharge composite.

there are new distinct features present, as shown by the broad shoulder at 1500 $cm^{-1}$ in the combined HiPco/PmPV spectrum, the combined spectrum appears to be doubly split. This shows that the composite is not simply an addition of the raw HiPco and pristine PmPV spectra. Figure 6 shows the combined raw arc discharge spectrum with the pristine polymer spectrum (A) and the 0.1% arc discharge composite (B). As with the HiPco combined spectrum, it is noted that the G line shift is due to a combination of both the raw arc discharge tubes and the pristine polymer. In both Figures 5 and 6, the composite spectrum is representative but can vary somewhat in profile from spot to spot on the sample. In no cases are the observed spectra a superposition of the spectra of the pristine materials. In Figure 6, the spectrum is almost dominated by the carbon nanotubes, and the peak of polymer origin at 1627 $cm^{-1}$ is absent.

Various authors have theoretically calculated the diameter dependence of the radial breathing mode frequency $\omega_{RBM}$ for isolated SWNTs and have used the functional form $\omega_{RBM}$ ($cm^{-1}$) $= A/d$ (nm) where $d$ is the SWNT diameter and $A$ is a constant. Using different methods, $A$ has been reported to be as small as 218 $cm^{-1}$ using a force-constant model[40] or as high as 236 $cm^{-1}$ using pseudopotential density functional theory,[41] with values of 223,[21] 227,[42] and 234 $cm^{-1}$ [43] also being reported. Experimentally, Jorio et al. have established a constant of 248 $cm^{-1}$ for isolated tubes based on the experimental assignment of 156 $cm^{-1}$ to a (13, 10) chiral tube at 785 nm on a $Si/SiO_2$ substrate.[32] The $\omega_{RBM}$ frequency is known to be upshifted by intertubule interaction in bundles.[23,44−47] Henrard et al. have proposed a tight-binding approach combined with a Lennard-Jones potential and have determined an 11% (∼22 $cm^{-1}$) upshift in the $\omega_{RBM}$ frequency for a (10, 10) bundle.[44] Venkateswaran et al. have reported a 7% (∼14 $cm^{-1}$) upshift for a (10, 10) bundle.[48] Kahn et al. have reported a 6% (∼12 $cm^{-1}$) increase for a (10, 10) bundle.[23] Kataura et al. have experimentally shown an increase of 4% (∼8 $cm^{-1}$) in the $\omega_{RBM}$ frequency when comparing Raman spectra of Br-doped and undoped nanotube samples.[47] In the following discussion, the constant $A$, which is closest to the mean (234 $cm^{-1}$ calculated using a local density approximation[43]) is used. This is similar to an approach taken by Bandow

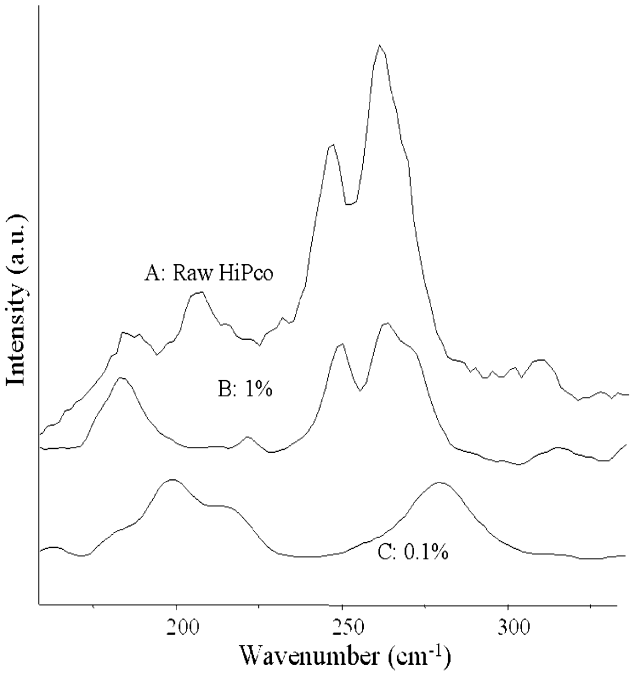


**Figure 7.** Raman spectra at 514.5 nm of various mass fractions of the HiPco composite.

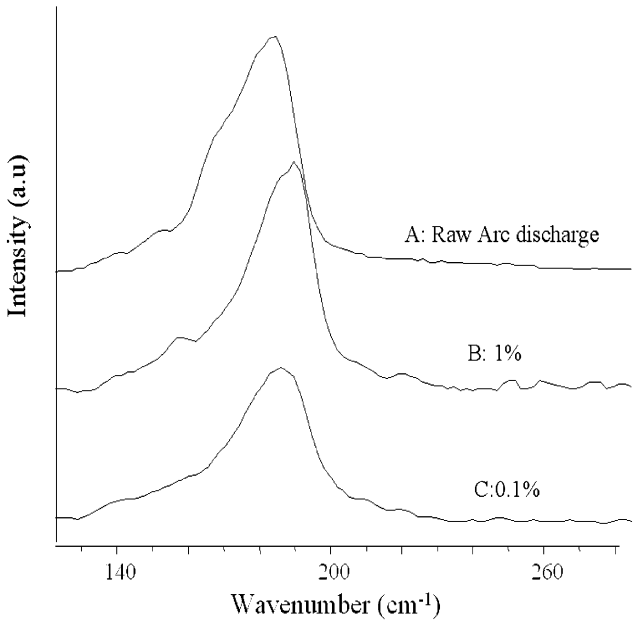


**Figure 8.** Raman spectra at 514.5 nm of various mass fractions of the arc discharge composite.

et al. which reduces the uncertainty in the diameters calculated from ±5 to 5%.[49] The 234-cm$^{-1}$ constant is modified to account for intertubule interaction in bundles to give $\omega_{RBM}$ (cm$^{-1}$) = 234/$d$ (nm) + 14 cm$^{-1}$. This value for the correction due to bundling is reported by Venkateswaran and was used because it is the closest to the mean for the values presented above. From additional analysis, authors have shown that the degree of upshift depends on the diameter of the tubes and the number of tubes present in the bundle.[33,44−45] This is not accounted for in the following discussion, but instead all modes are calculated on the basis of the shifting of a (10, 10) tube, which has a diameter of 1.37 nm which is close to the mean diameter in the arc discharge sample (1.42 cm$^{-1}$) as seen in the UV/vis/NIR. Because HiPco and arc discharge tubes have different diameter distributions, in the following discussion the modified Kürti model is employed to determine diameters from the spectra of the raw arc discharge nanotubes. The Kukovecz model is applied to determine the diameters present in the HiPco samples where $\omega_{RBM}$ (cm$^{-1}$) = 239/$d$ (nm) + 8.5 cm$^{-1}$.[34] This value is complicated further in the composites because of the presence of the polymer. In the spectra of the composites, peaks that are obviously shifted from their positions within the raw material are assigned to the same diameters. Thus, this has been modified for arc discharge composites to be $\omega_{RBM} = (234/d\ (\text{nm})) + \Gamma$ or for HiPco composites to be $\omega_{RBM} = (239/d\ (\text{nm})) + \Gamma$ where $\Gamma$ represents the diameter-independent approximation resulting from the environment of the tubes and is 14 cm$^{-1}$ for raw arc discharge soot and 8.5 cm$^{-1}$ for HiPco soot. For polymer-tube systems, $\Gamma$ is estimated to be 21 cm$^{-1}$ for arc discharge composites[7] and 11.5 cm$^{-1}$ for HiPco composites. Previous reports on PMMA and arc discharge composites have estimated an upshift of 20 cm$^{-1}$ for low concentrations (0.5% mass fractions).[50]

Figure 7 shows the radial breathing modes (RBM) of different loading fractions of HiPco SWNTs within polymer composites at an excitation wavelength of 514.5 nm. Curve A shows the raw HiPco SWNT sample. Both metallic and semiconducting tubes are resonant, similar to the G line of the raw HiPco spectrum presented in Figure 3. There are five distinct peaks present. The dominant metallic modes occur at 261, 246, and 312 cm$^{-1}$. Using the relationship outlined above for raw HiPco soot, $\omega_{RBM} = (239/d\ (\text{nm})) + 8.5$ cm$^{-1}$, which correspond to nanotube diameters of 0.95, 1.00, and 0.79 nm. Also resonant are semiconducting tubes at 186 and 206 cm$^{-1}$, which correspond to nanotube diameters of 1.33 and 1.20 nm. This diameter distribution is similar to that of the HiPco RBM spectra presented previously.[34] It has been suggested that HiPco contains more structured strong peaks both at low and high wavenumbers compared to arc discharge RBM spectra; therefore, a more complex diameter distribution that could be a broader monomodal Gaussian is required.[34] Kukovecz et al. have used an experimentally derived monomodal Gaussian distribution to determine a diameter distribution of 0.73−1.23 nm[34] for HiPco tubes, and Zhou et al. have determined a diameter distribution of 0.8−1.4 nm for HiPco tubes.[17]

Curve B shows the 1% HiPco composite. Also present here are five distinct features. The two dominant $\omega_{RBM}$ peaks have both upshifted by 3 cm$^{-1}$ to 249 and 264 cm$^{-1}$ and are at the same relative intensity, unlike the situation in the raw sample. Peaks are also present at 189 and 209 cm$^{-1}$, with the emergence of a new peak at 217 cm$^{-1}$ corresponding to a nanotube diameter of 1.15 nm, using the relationship of $\omega_{RBM} = (239/d\ (\text{nm})) + 11.5$ cm$^{-1}$ as stated above for HiPco composites. This size selection has also been reported for arc discharge/PmPV composites.[7] Curve C shows the 0.1% HiPco composite with the dominant peak occurring at 198 cm$^{-1}$, which corresponds to a nanotube diameter of 1.27 nm. Also present is the peak at 217 cm$^{-1}$ that also occurs at the 1% loading fraction but is more pronounced at the 0.1% loading fraction. The third peak occurs at 186 cm$^{-1}$, which corresponds to a diameter of 1.35 nm. A refinement in the smaller-diameter nanotubes is seen with only a peak corresponding to a diameter of 0.98 nm present, which does not appear to be present at 1% mass fraction. This marries well with the G line data which suggest that the solubility limits of the composite occur between 0.1 and 1%. Figure 8 shows the $\omega_{RBM}$ of different loading fractions of arc discharge SWNTs within polymer composites at 514.5 nm. Curve A shows the raw arc discharge RBM spectrum, which is dominated by

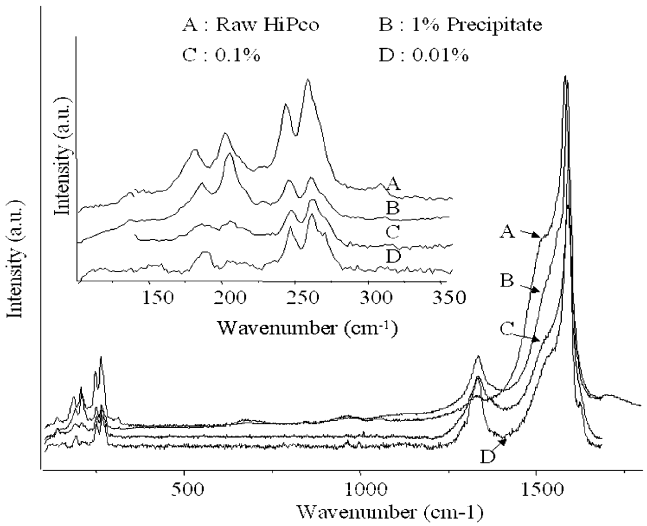


**Figure 9.** Raman spectra at 514.5 nm of the HiPco/PmPV precipitate.

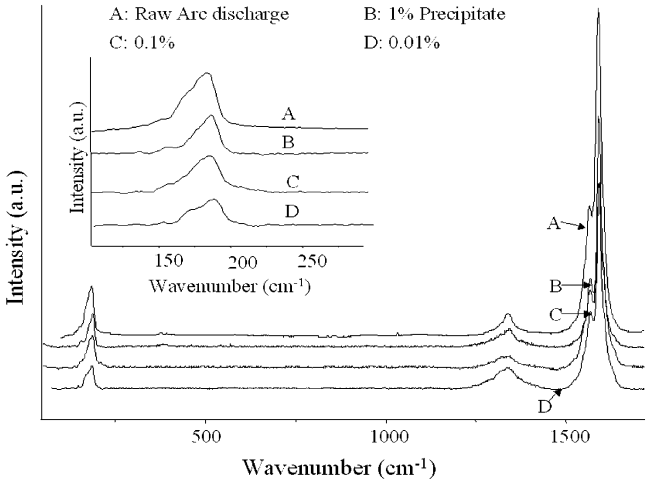


**Figure 10.** Raman at 514.5 nm of the arc discharge/PmPV precipitate.

semiconducting tubes. Modes are resonant at 185, 178, 167, and 155 $cm^{-1}$. These peaks correspond to diameters of 1.34, 1.39, 1.48, and 1.6 nm calculated using the relationship presented earlier: $\omega_{RBM} = (234/d\ (nm)) + 14\ cm^{-1}$. The RBM spectra presented here are similar to previously reported spectra for arc discharge.[15] The resonant Raman effect is clearly seen here because this diameter distribution is considerably smaller than that seen in the NIR spectrum in Figure 2. This also explains the smaller fwhm of the raw arc discharge G line compared to that of the raw HiPco G line as seen in Figures 3 and 4. In the 1% arc discharge composite, the shoulder corresponding to the 1.56 nm tube is no longer present, and the dominant peak has shifted by 7 $cm^{-1}$ to 192 $cm^{-1}$, which corresponds to a diameter of 1.34 nm. A 1.64 nm nanotube is also present at this mass fraction, as well as a new feature at 220 $cm^{-1}$ corresponding to a tube diameter of 1.16 nm. As the mass fraction is reduced further to 0.1%, it can be seen that the most dominant peak is still in the same position at 192 $cm^{-1}$, with a shoulder at 200 $cm^{-1}$ present, which corresponds to a diameter of 1.28 nm. The peak at 159 $cm^{-1}$ is no longer resonant, but a shoulder at 168 $cm^{-1}$ corresponding to a diameter of 1.52 nm is observed. Thus, which nanotubes have remained in solution has been established.

The precipitate was investigated to determine what fell out of both composite solutions. Figure 9 presents the 514.5 nm Raman spectra of the precipitate of the various mass fractions of the HiPco composite as well as the raw HiPco spectrum. From the RBM data obtained at 514.5 nm, it is observed that nanotube diameters of 1.33 and 1.2 nm decreases in intensity as the mass fraction is lowered and are no longer present in the filtrate at 0.01%. This would suggest that these tube diameters were selected by the polymer because they are not present in the precipitate. This agrees well with the RBM spectrum presented earlier in Figure 7, which shows a refined selection of the smaller tubes and is dominated by larger tubes. The larger-diameter, semiconducting SWNTs are more abundant in the 1% precipitate (B), and the 0.1 and 0.01% HiPco precipitates are dominated by smaller metallic tubes; this would explain their reduction in the composite spectrum at 0.1%. There are significant changes in the G line with a decrease in the fwhm as the mass fraction of the tubes decreases. This shows that the reduction in the diameter distribution is similar to that of the composite sample. However, it is noted that the 0.1% and 0.01% G line precipitates are more tubelike compared to the composite which is more polymerlike. This could explain the difficulty in getting a 0.01% composite spectrum at 514.5 nm.

Figure 10 presents Raman spectra at 514.5 nm for the various mass fractions of the arc discharge PmPV precipitate. In the RBM region in Figure 10, we note that the precipitate spectrum is similar to the composite spectra in Figure 8. This suggests that the arc discharge tubes are not mutually exclusive with respect to the composite or the precipitate because similar nanotubes appear in both. The situation is different in Figure 9 because larger-diameter semiconducting SWNTs are relatively better represented in the precipitate than in the raw sample and are almost absent in the 0.1% sample, which is a good signal for metallic tubes. Like the HiPco G line precipitate, the arc discharge G line is more tubelike at 0.1 and 0.01% compared to the composite. This suggests that more tubes that are resonant at 514.5 nm have fallen out at the lower mass fractions. In conclusion, it was shown that PmPV interacts with both HiPco and arc discharge tubes. A degree of selectivity at 1% mass fraction was shown for both tubes in the UV/vis/NIR. The raw HiPco has a diameter distribution of 0.73 to 1.5 nm in the UV/vis/NIR, and the 1% composite has a diameter distribution of 0.8 to 1.35 nm. A similar reduction in the diameter range was seen in the 1% arc discharge composite UV/vis/NIR spectrum, where a diameter distribution of 1.1 to 1.74 nm was reduced from 1.16 to 1.6 nm in the 1% arc discharge composite. This was reduced further from 1.32 to 1.6 nm in the 0.01% arc discharge composite. The Raman spectrum of the HiPco 0.1% composite shows tubes with diameters of 1.34, 1.26, and 1.15 nm being selected. The Raman spectrum of the 0.1% arc discharge composite shows tubes of 1.51, 1.34, and 1.28 nm being selected.

Table 1 presents possible assignment of tubes, which could be resonant at 514.5 nm. These assignments are made using the model in ref 51 where $\alpha_{c-c}$, the nearest-neighbor carbon−carbon distance, is 0.144 nm and $\gamma_0$ is 2.9 eV,[52] which is the nearest-neighbor carbon−carbon interaction energy. A damping factor of 11.5 $cm^{-1}$ is employed for HiPco composites, and 21 $cm^{-1}$ is employed for arc discharge composites, as observed in Figures 4 and 5. RBM assignments indicate that PmPV appears to be interacting predominantly with semiconducting arc discharge tubes, whereas both metallic and semiconducting HiPco tubes resonate at 514.5 nm. The G line of both the arc discharge tubes and HiPco tubes do not show dominant metallic contributions at the 0.1 and 0.01% mass fractions. Typical metallic G-line contributions consist of a higher-frequency mode that is Lorentzian in shape, whereas the lower-frequency mode

**TABLE 1: Assignment of Some Possible Chiralities Present at 514.5-nm Laser Excitation for the 0.1% Mass Fraction HiPco Composite and the 0.1% Mass Fraction Arc Discharge Composite**

| 0.1% HiPco | | | | 0.1% arc discharge | | | |
|---|---|---|---|---|---|---|---|
| *d* (nm) | $C_h$ (*n*, *m*) | type | electronic properties | *d* (nm) | $C_h$ (*n*, *m*) | type | electronic properties |
| 0.98 | (10, 4) | chiral | metallic | 1.27 | (15, 2) | chiral | semiconducting |
| 1.15 | (14, 2) | chiral | metallic | | (16, 0) | zigzag | semiconducting |
| 1.27 | (16, 0) | zigzag | semiconducting | | (13, 5) | chiral | semiconducting |
| | (13, 5) | chiral | semiconducting | | (14, 4) | chiral | semiconducting |
| | (14, 4) | chiral | semiconducting | 1.34 | (17, 0) | zigzag | semiconducting |
| | (15, 2) | chiral | semiconducting | | (11, 9) | chiral | semiconducting |
| 1.35 | (13, 6) | chiral | semiconducting | | (13, 6) | chiral | semiconducting |
| | (11, 9) | chiral | semiconducting | | (15, 4) | chiral | semiconducting |
| | (17, 0) | zigzag | semiconducting | 1.51 | (15, 7) | chiral | semiconducting |
| | (15, 4) | chiral | semiconducting | | (17, 3) | chiral | semiconducting |

[a] $a_{c-c} = 0.144$ nm, $\gamma_0 = 2.9$ eV,[52] and $\omega_{RBM}$ (cm$^{-1}$) = 234/*d* (nm) + 21 cm$^{-1}$ for arc discharge composites;[43] $\omega_{RBM}$ (cm$^{-1}$) = 239/*d* (nm) + 11.5 cm$^{-1}$ for HiPco composites.[34] *d* refers to corresponding diameters, and $C_h$ refers to chiral vectors described in ref 1.

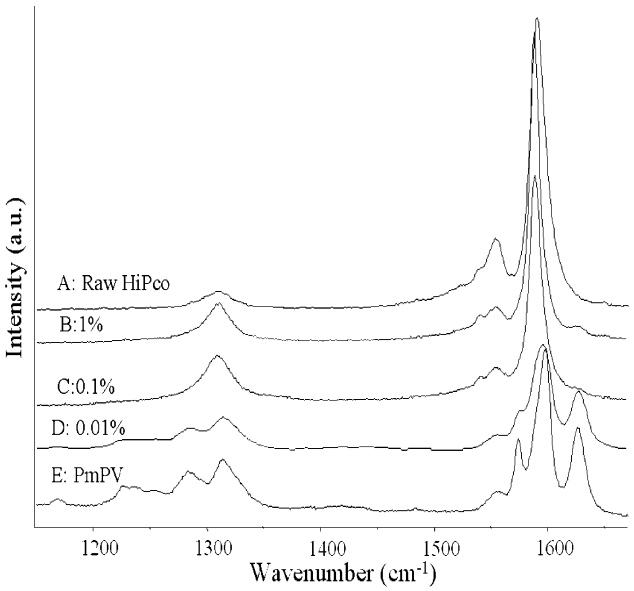


**Figure 11.** Raman spectra at 632.8 nm of various mass fractions of the HiPco composite.

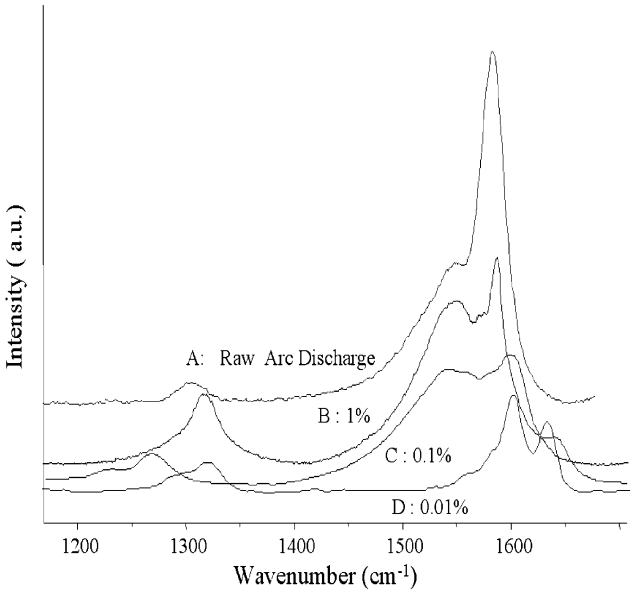


**Figure 12.** Raman spectra at 632.8 nm of various mass fractions of the arc discharge composite.

exhibits an asymmetric Breit−Wigner−Fano line shape as seen in the 1% HiPco composite.[27] This could explain why so few arc discharge tubes are resonant at 514.5 nm and more HiPco's are resonant at 514.5 nm, as seen in the RBMs of both of these composites. It has been shown that PmPV interacts with both arc discharge and HiPco tubes in the diameter region of 0.98 to 1.51 nm, and these tubes appear to be predominantly semiconducting in nature when excited using a 514.5-nm laser. However, it must be stated that within this diameter region semimetallic arc discharge tubes are predominantly resonant at 514.5 nm.

Figures 11 and 12 present the G line regions of the HiPco and arc discharge composites at 632.8 nm. First, we note that the G line of the HiPco composite at 514.5 nm is distinctly different from that at 632.8 nm and that the arc discharge composite at 514.5 nm is distinctly different from that at 632.8 nm. These G-line spectra clearly show the resonance Raman effect. In Figures 11 and 12, similar shifts in the G line as shown previously at 514.5 nm are seen here using a laser excitation of 632.8 nm. However, it is clearly seen that the 1 and 0.1% mass fractions of both the HiPco and arc discharge composite spectra are distinctly different.

The UV/vis/NIR of the raw arc discharge spectrum shows a diameter distribution of 1.1−1.74 nm. At 632.8 nm, semiconducting tubes around ∼1.55 nm are expected to resonate, and metallic tubes around ∼1.3 nm are expected to resonate according to resonance Raman theory.[19,53] However, the G line of the raw arc discharge spectrum shows strong semiconducting contributions. As the mass fraction is lowered, the BWF line shape is especially seen at the 0.1% mass fraction, and this has been reported previously for raw arc discharge samples.[27] This would suggest that PmPV is interacting preferentially with the smaller metallic tubes around ∼1.3 nm. However, because both the 0.1 and 0.01% arc discharge spectra have significant contributions from the pristine polymer, it is difficult to estimate the relative contributions of the metallic tubes. The UV/vis/NIR of the raw HiPco spectrum shows a diameter distribution of 0.73−1.5 nm. Tubes around ∼0.8 and ∼1.55 nm are expected to be semiconducting, but tubes around ∼1.3 nm are expected to be metallic. In Figure 11, the HiPco composite is dominated by semiconducting contributions, which are composed of four to five Lorentzian components. This shows that PmPV is not prejudiced toward tube type. The RBMs of the corresponding G lines are presented in Figures 13 and 14.

In Figure 13, the HiPco composite spectra are presented. A broad range of diameters from 0.84 to 1.54 nm is seen here in the raw HiPco spectrum, with diameters of 0.88, 0.98, 1.15, and 1.29 nm also resonating. The raw HiPco sample is dominated by the 0.98 nm tube, and the 0.1 and 0.01% composites are dominated by the 1.29 nm tube. This is similar

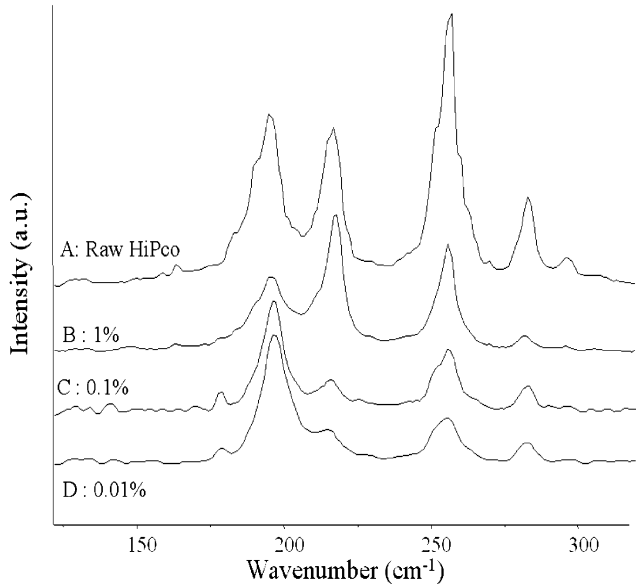


**Figure 13.** Raman spectra at 632.8 nm of various mass fractions of the HiPco composite.

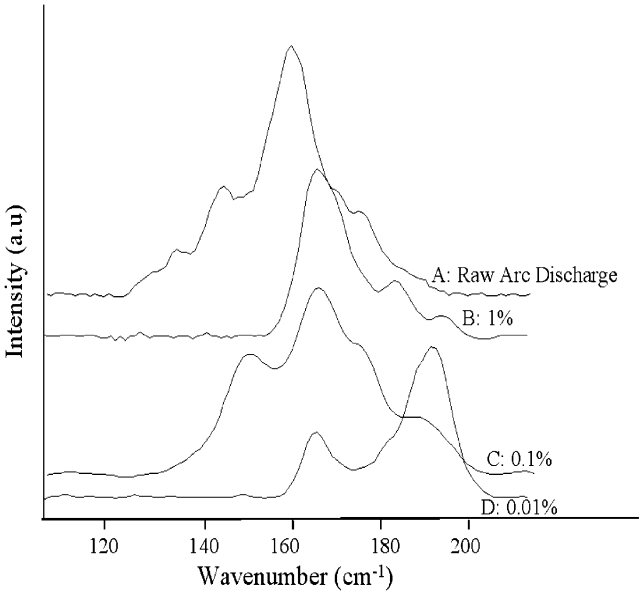


**Figure 14.** Raman spectra at 632.8 nm of various mass fractions of the arc discharge composite.

to what is seen at 514.5 nm for the HiPco composite. A peak is also present at 1.15 nm but is less enhanced; it also appears at 514.5 nm. However, at laser excitation of 632.8 nm the latter is likely to be metallic. Metallic tubes dominate the RBM spectrum of the HiPco composite, but semiconducting tubes dominate the corresponding G-line composite spectra. This is possible because the resonance condition for $\omega_{RBM}$ differs from that for the G band by the G-band phonon energy ($\sim$0.2 eV).[54] In Figure 14, the arc discharge composite spectra are shown. Curve A shows the raw arc discharge sample. Here multiple modes are centered on the most dominant mode at 161 $cm^{-1}$ corresponding to a diameter of 1.54 nm, with diameters as large as 1.72 nm and as small as 1.32 nm present. The three composites in Figure 14 at 1, 0.1, and 0.01% all have two similar peaks present corresponding to diameters of 1.54 and 1.32 nm. It is likely that the 1.54-nm tube is semiconducting, possibly a (20, 0) zigzag tube, a (12, 11) tube, or (16, 6) chiral tube. However, it is likely that the 1.32-nm tube is metallic, possibly a (16, 1) or a (15, 3) chiral tube.

## 4. Conclusions

This work attempts to show that PmPV interacts with both HiPco SWNTs and arc discharge SWNTs and that this interaction is more diameter-selective than tube-type-selective. The UV/vis/NIR of both the HiPco composite and the arc discharge composite at 1% mass fraction by weight shows a degree of selectivity. This interaction is further investigated using Raman spectroscopy. From the $\omega_{RBM}$ of both the arc discharge and HiPco composites at 514.5 and 632.8 nm, a variety of semiconducting and metallic tubes are selected. Although only two excitation wavelengths are employed, it is noted that in the 0.1 and 0.01% HiPco composites the larger tubes dominate the spectra whereas in the 0.1 and 0.01% arc discharge composite spectra the smaller-diameter tubes dominate the spectra. However, similar diameters of $\sim$1.27 and $\sim$1.35 nm are selected in both composites. Furthermore, the G lines for both the HiPco and the arc discharge composites appear to show semiconducting and metallic contributions. This suggest that the polymer is not tube-type-selective but is more likely to be diameter-selective because similar diameter ranges are selected at both wavelengths. Further analysis using alternative wavelengths could help reinforce these findings.

**Acknowledgment.** We thank FOCAS, which is funded under the National Development Plan 2000-2226 with assistance from the European Regional Development Fund. S.M.K. acknowledges DIT scholarship support, GDPC, the University of Montpellier Π, Montpellier, France for arc discharge nanotubes, and Trinity College Dublin for PmPV.

## References and Notes

(1) Saito, R.; Dresselhaus, G.; Dresselhaus, M. S. *Physical Properties of Carbon Nanotubes*; Imperial College Press: London, 1999.

(2) Rao, C. N. R.; Satishkumar, B. C.; Govindaraj, A.; Nath, M. *ChemPhysChem* **2001**, *2*, 78.

(3) Thess, A.; Lee, R.; Nikolaev, P.; Dai, H. J.; Petit, P.; Robert, J.; Xu, C. H.; Lee, Y. H.; Kim, S. G.; Rinzler, A. G.; Colbert, D. T.; Scuseria, G. E.; Tomanek, D.; Fischer, J. E.; Smalley, R. E. *Science* **1996**, *273*, 483.

(4) Journet, C.; Maser, W. K.; Bernier, P.; Loiseau, A.; De La Chapelle, M. L.; Lefrant, S.; Deniard, P.; Lee, R.; Fischer, J. E. *Nature* **1997**, *388*, 756.

(5) Nikolaev, P.; Bronikowski, M. J.; Kelley Bradley, R.; Rohmund, F.; Colbert, D. T.; Smith, K. A.; Smalley, R. E. *Chem. Phys. Lett.* **1999**, *313*, 91.

(6) Chiang, I. W.; Brinson, B. E.; Haung, A. Y.; Willis, P. A.; Bronikowski, M. J.; Margrave, J. L.; Smalley, R. E.; Hague, R. H. *J. Phys. Chem. B* **2001**, *105*, 8297.

(7) Dalton, A. B.; Stephan, C.; Coleman, J. N.; Ajayan, P. M.; Lefrant, S.; Bernier, P.; Blau, W. J.; Byrne, H. J. *J. Phys. Chem. B* **2000**, *104*, 10012.

(8) Panhuis, M. I. H.; Munn, R. W.; Blau, W. J. *Synth. Met.* **2001**, *121*, 1187.

(9) Panhuis, M. I. H.; Maiti, A.; Dalton, A. B.; Van Der Noort, A.; Coleman, J. N.; McCarthy, B.; Blau, W. J. *J. Phys. Chem. B* **2003**, *107*, 478.

(10) Dalton, A. B.; Coleman, J. N.; Panhuis, M. I. H.; McCarthy, B.; Drury, A.; Blau, W. J.; Paci, B.; Nunzi, J.-N.; Byrne, H. J. *J. Photophys. Photochem. A: Chem.* **2001**, *5678*, 1.

(11) Coleman, J. N.; Fleming, A.; Maier, S.; O'Flaherty, S.; Minett, A. I.; Ferreira, M. S.; Hutzler, S.; Blau, W. J. *J. Phys. Chem. B* **2004**, *108*, 3446.

(12) McCarthy, B.; Coleman, J. N.; Czerw, R.; Dalton, A. B.; Carroll, D. L.; Blau, W. J. *Synth. Met.* **2001**, *121*, 1225.

(13) Steuerman, D. W.; Star, A.; Narizzano, R.; Choi, H.; Ryan, S. R.; Nicolini, C.; Stoddart, J. F.; Heath, J. R. *J. Phys. Chem. B* **2002**, *106*, 3124.

(14) Lefrant, S.; Baltog, I.; Lamy de la Chapelle, M.; Baibarac, M.; Louarn, G.; Journet, C.; Bernier, P. *Synth. Met.* **1999**, *100*, 13.

(15) Stephan, C.; Nguyen, T. P.; Lamy de la Chapelle, M.; Lefrant, S.; Journet, C.; Bernier, P. *Synth. Met.* **2000**, *108*, 139.

(16) Shi, Z.; Lian, Y.; Zhou, X.; Gu, Z.; Zhang, Y.; Iijima, S.; Zhou, L.; Yue, K. T.; Zhang, S. *Carbon* **1999**, *38*, 1449.

(17) Zhou, W.; Ooi, Y. H.; Russo, R.; Papanek, P.; Luzzi, D. E.; Fischer, J. E.; Bronikowski, M. J.; Willis, P. A.; Smalley, R. E. *Chem. Phys. Lett.* **2001**, *350*, 6.

(18) Journet, C.; Bernier, P. *Appl. Phys. A* **1998**, *67*, 1.
(19) Kataura, H.; Kumazawa, Y.; Maniwa, Y.; Umeza, I.; Suzuki, S.; Ohtsuka, Y.; Achiba, Y. *Synth. Met.* **1999**, *103*, 2555.
(20) Hagan, A.; Hertel, T. *Nano Lett.* **2003**, *3*, 383.
(21) Rao, A. M.; Richter, E.; Bandow, S.; Chase, B.; Eklund, P. C.; Williams, K. A.; Fang, S.; Subbaswamy, K. R.; Menon, M.; Thess, R. E.; Dresselhaus, G.; Dresselhaus, M. S. *Science* **1997**, *275*, 187.
(22) Keogh, S. M.; Maguire, A.; Hedderman, T. G.; Gregan, E.; Farrell, G.; Dalton, A. B.; McCarthy, B.; Chambers, G.; Byrne, H. J. *Proc. SPIE Int. Soc. Opt. Eng.* **2002**, *4876*, 723.
(23) Kahn, D.; Lu, J. P. *Phys. Rev. B* **1999**, *60*, 6535.
(24) Saito, R.; Takeya, T.; Kimura, T.; Dresselhaus, G.; Dresselhaus, M. S. *Phys. Rev. B* **1998**, *57*, 4145.
(25) Jorio, A.; Dresselhaus, G.; Dresselhaus, M. S.; Souza, M.; Dantas, M. S. S.; Pimenta, M. A.; Rao, A. M.; Saito, R.; Liu, C.; Cheng, H. M. *Phys. Rev. Lett.* **2000**, *85*, 2617.
(26) Pimenta, M. A.; Marucci, A.; Empedocles, S. A.; Bawendi, M. G.; Hanlon, E. B.; Rao, A. M.; Eklund, P. C.; Smalley, R. E.; Dresselhaus, G.; Dresselhaus, M. S. *Phys. Rev. B* **1998**, *58*, 16016.
(27) Brown, S. D. M.; Jorio, A.; Corio, P.; Dresselhaus, M. S.; Dresselhaus, G.; Saito, R.; Kneipp, K. *Phys. Rev. B* **2001**, *63*, 155414.
(28) Dubay, O.; Kresse, G.; Kutzmany, H. *Phys. Rev. Lett.* **2002**, *88*, 235506.
(29) Jorio, A.; Souza Filho, A. G.; Dresselhaus, G.; Dresselhaus, M. S.; Swan, A. K.; Unlu, M. S.; Goldberg, B. B.; Pimenta, M. A.; Hafner, J. H.; Lieber, C. M.; Saito, R. *Phys. Rev. B* **2002**, *65*, 155412.
(30) Bendiab, N.; Almairac, R.; Paillet, M.; Sauvajol, J. L. *Chem. Phys. Lett.* **2003**, *372*, 210.
(31) Jiang, C.; Kempa, K.; Zhoa, J.; Schlecht, U.; Kolb, U.; Basche, T.; Burghard, M.; Mews, A. *Phys. Rev. B* **2002**, *66*, 161404.
(32) Jorio, A.; Saito, R.; Hafner, J. H.; Lieber, C. M.; Hunter, M.; McClure, T.; Dresselhaus, G.; Dresselhaus, M. S. *Phys Rev. Lett.* **2001**, *86*, 1118.
(33) Kuzmany, H.; Plank, W.; Hulman, M.; Gruneis, A.; Pichler, T.; Peterlik, H.; Kataura, H.; Achiba, Y. *Eur. Phys. J. B* **2001**, *22*, 307.
(34) Kukovecz, A.; Kramberger, C.; Georgakilas, V.; Prato, M.; Kuzmany, H. *Eur. Phys. J. B* **2002**, *28*, 223.
(35) Dalton, A. B. Ph.D. Thesis, Dublin University, Dublin, Ireland, 1999; Chapter 5.
(36) Tian, B.; Zerbi, G.; Schenk, R.; Mullen, K. *J. Chem. Phys.* **1991**, *96*, 3191.
(37) Buisson, J. P.; Lefrant, S.; Mevellec, J. Y.; Orion, I.; Eckhardt, H. *Synth. Met.* **1992**, *49*, 305.
(38) Orion, I.; Buisson, J. P.; Lefrant, S. *Phys. Rev. B* **1998**, *57*, 4050.
(39) Hedderman, T. G.; O Neill, L.; Maguire, A.; Keogh, S. M.; Gregan, E.; McCarthy, B.; Dalton, A. B.; Chambers, G.; Byrne, H. J. *Proc. SPIE Int. Soc. Opt. Eng.* **2002**, *4876*, 696.
(40) Jishi, R. A.; Venkataraman, L.; Dresselhaus, M. S. *Chem. Phys. Lett.* **1993**, *209*, 77.
(41) Sanchez-Portal, D.; Artacho, E.; Soler, J. M.; Rubio, A.; Ordejon, P. *Phys. Rev. B* **1998**, *58*, R8869.
(42) Mahan, G. D. *Phys. Rev. B* **2002**, *65*, 235402.
(43) Kürti, J.; Kresse, G.; Kuzmany, H. *Phys. Rev. B* **1998**, *58*, R8869.
(44) Henrard, L.; Popov, V. N.; Rubio, A. *Phys. Rev. B* **2001**, *64*, 205402.
(45) Henrard, L.; Hernandez, E.; Bernier, P.; Rubio, A. *Phys. Rev. B* **1999**, *60*, 8521.
(46) Rao, A. M.; Chen, J.; Richter, E.; Schlecht, U.; Eklund, P. C.; Haddon, R. C.; Venkateswaran, U. D.; Kwon, Y. K.; Tomanek, D. *Phys. Rev. Lett.* **2001**, *86*, 3895.
(47) Kataura, H.; Maniwa, Y.; Masubuchi, S.; Kazama, S.; Zhao, X.; Ando, Y.; Ohtsuka, Y.; Suzuki, S.; Achiba, Y.; Saito, R. *Electronic Properties of Novel Materials: Molecular Nanostructures*, XIV International Winterschool/Euroconference; Kuzmany, H., et al. Ed.; Kirchberg, 2000; p 262.
(48) Venkateswaran, U. D. *Phys. Rev. B* **1999**, *59*, 10928.
(49) Bandow, S.; Chen, G.; Sumanasekera, G. U.; Gupta, R.; Yadasaka, N.; Iijima, S.; Eklund, P. C. *Phys. Rev. B* **2000**, *66*, 075416.
(50) Lefrant, S.; Buisson, J. P.; Schreiber, J.; Chauvet, O.; Baibarac, M.; Baltog, I. *Synth. Met.* **2003**, *391*, 783.
(51) Yu, Z.; Brus, L. *J. Phys. Chem. B* **2001**, *105*, 1123.
(52) Milneara, M.; Kürti, J.; Hulman, M.; Kuzmany, H. *Phys. Rev. Lett.* **2000**, *84*, 1324.
(53) Wang, W. F.; Cao, X. W.; Hu, S. F.; Liu, Y. Y.; Lan, G. X. *Chem. Phys. Lett.* **2001**, *336*, 47.
(54) Saito, R.; Jorio, A.; Hafner, J. H.; Lieber, C. M.; Hunter, M.; McClure, T.; Dresselhaus, G.; Dresselhaus, M. S. *Phys. Rev. B* **2001**, *64*, 085312.